



ELSEVIER

Available online at www.sciencedirect.com

SCIENCE @ DIRECT®

Medical Image Analysis xxx (2005) xxx–xxx

**MEDICAL  
IMAGE  
ANALYSIS**

www.elsevier.com/locate/media

## Towards a realistic echographic simulator

D. d'Aulignac<sup>a</sup>, C. Laugier<sup>a,\*</sup>, J. Troccaz<sup>b</sup>, S. Vieira<sup>a</sup>

<sup>a</sup> INRIA Rhône Alpes & GRAVIR, 38330 Montbonnot, France

<sup>b</sup> TIMC-IMAG, 38706 La Tronche, France

Received 20 May 2003; received in revised form 31 August 2004; accepted 22 February 2005

### 8 Abstract

9 Echography is a useful tool to diagnose a thrombosis; however, since it is difficult to learn to perform this procedure, the objective of this work is to create a simulation to allow students to practice in a virtual environment.

11 Firstly, a physical model of the thigh was constructed based on experimental data obtained using a force sensor mounted on a robotic arm. We present a spring damper model consisting of both linear and non-linear elements. The parameters of each of these elements are then fitted to the experimental data using an optimization technique. By employing an implicit integration to solve the dynamics of the system we obtain a stable physical simulation at over 100 Hz.

15 Secondly, a haptic interface was added to interact with the simulation. Using a PHANTOM force-feedback device may touch and deform the thigh in real-time. In order to allow a realistic sensation of the contact we employ a local modeling technique allowing to approximate the forces at much higher frequency using a multi-threaded architecture.

17 Finally, we present the basis for a fast echographic image generation depending on the position and orientation of the virtual probe as well as the force applied to it.

19 © 2005 Published by Elsevier B.V.

21

### 22 1. Introduction

23 A very useful exam is the echography of the thigh to detect a thrombosis in the vein. A healthy vein will compress under the influence of an external force while a vein affected by thrombosis will only partially or even not at all compress, depending on the stage in the evolution of the illness. Depending on the pressure the practitioner applies with the echographic probe on the thigh, he will get an image from which the current state of the vein can be deduced, and hence a possible thrombosis diagnosed.

33 *Motivations.* However, the learning process of this procedure is somehow long and only after approxi-

24 mately 1000 echographic exams an acceptable competence in acquired. The first 500 exams will have to be carried out under the supervision of an experienced practitioner. Virtual environments present an alternative to the conventional medical training scheme. It is possible to create an interactive 3D simulation environment, where the doctors can manipulate or cut virtual models of organs and tissues with a haptic interface. The idea is similar to using flight simulators to train pilots. Virtual environments give an environment where there is no risk to a patient, and therefore less stressful. They are interactive and three dimensional contrary to books. Virtual environments also give a unique advantage, as it is possible to generate arbitrary anatomies and pathologies, so that the doctors can be trained for cases that are not frequently encountered.

50 *Objectives.* The goal of this work is to lay the groundwork for the development of an echographic simulator 51 52

\* Corresponding author.

E-mail addresses: diego@aulignac.com (D. d'Aulignac), christian.laugier@inrialpes.fr (C. Laugier), jocelyne.troccaz@imag.fr (J. Troccaz).

53 with force feedback. In the final system, the trainee will  
54 be looking at artificially generated echographic images,  
55 and interacting with a computer simulated dynamical  
56 thigh model through a haptic interface. Constructing  
57 realistic but computationally efficient models is the main  
58 challenge in developing a virtual reality training simula-  
59 tor. In this application it is necessary to have models for  
60 deformable tissue being manipulated by the doctor as  
61 well as models to construct artificial echographic  
62 images.

63 In this paper, a dynamic model of the human thigh  
64 based on experimentally determined deformation char-  
65 acteristics will be presented, followed by a discussion  
66 of the results and future directions.

## 67 2. Previous work

### 68 2.1. Echographic image generation

#### 69 2.1.1. Generative approach

70 Ultrasound imaging is based on ultrasonic wave  
71 propagation inside matter. The generative approach is  
72 a physical approach consisting in modeling this propa-  
73 gation. Therefore, in order to generate images, we need  
74 accurate physical and geometrical models of both the  
75 probe (characteristics of emitters and receptors) and tis-  
76 sues to be observed. We need also a model of the inter-  
77 action between the acoustic wave and the tissues. This is  
78 a very complex problem which can be tackled in several  
79 ways depending on the objectives of the simulation.

80 Meunier has focused on the simulation of echocar-  
81 diographic image textures (Meunier, 1989). The purpose  
82 is here to be able to automatically recognize tissues from  
83 the texture analysis of the image. His study is based on  
84 Bamber and Dickinson work (Bamber and Dickinson,  
85 1986) concerning diffuser modeling. However, generat-  
86 ing a realistic ultrasound image needs a more complete  
87 modeling. Jensen has taken into account the ultrasonic  
88 wave behavior at interfaces and the geometry of the ana-  
89 tomical structures. He has generated an ultrasound im-  
90 age of a cyst (Jensen, 1996). The computation of this  
91 image, including only two kinds of structures, has lasted  
92 11 h! Varlet proposes an attractive solution dealing with  
93 real-time constraints (Varlet, 1997). Firstly, a 3D model  
94 of organs is built from CT or MRI data (e.g., from the  
95 Visible Human Project) using implicit surfaces. Then,  
96 for a given position of the echographic probe, the image  
97 is generated using a ray tracing method adapted to ultra-  
98 sonic rays. In order to reduce the computational time,  
99 propagation and reflection are the only acoustical prop-  
100 erties that are considered at a purely geometric level.  
101 Texture-less images displaying the tissue interfaces are  
102 generated for echo-endoscopic applications. In these  
103 applications a major issue is to understand the topogra-  
104 phy of the organs from the echographic images to be

able to monitor the difficult progression of the endo- 105  
scope in the gastrointestinal track. Work is in progress 106  
to map textures onto these images. Wibaux et al. 107  
(1997) generated echographic images directly from the 108  
geometric model of the anatomy. The echographic proc- 109  
ess itself is simulated by modeling the refraction of the 110  
signal caused by the organs. In the quest for real-time 111  
performance a simplified refraction model is used to 112  
generate the images. 113

Generative approaches have the advantage of being 114  
applicable to any type of organs provided that a model 115  
of them is available. However, we have shown that the 116  
acoustic phenomena to be rendered are extremely com- 117  
plex and even simplified simulation is very time-consum- 118  
ing. In our context, where real-time simulation is needed, 119  
a large computational time is totally prohibitive. The 120  
compromise which has been proposed by Varlet (1997) 121  
reduces the computing time but does not allow yet to 122  
generate textured images which is prohibitive for most 123  
clinical application of echography. 124

#### 2.1.2. Interpolation approach 125

An effective alternative to the generative approach is 126  
to require a more or less dense 3D ultrasound volume 127  
from which images can be generated. The 3D ultrasound 128  
volume is acquired in an off-line pre-processing and 129  
images are generated during simulation, by computing 130  
a slice in the volume. Such images can be generated very 131  
rapidly. As they come from real ultrasound images, 132  
there is no realism problem. Aiger from Tel-Aviv univer- 133  
sity presents UltraSim, a commercial real-time ultra- 134  
sound simulator (Aiger and Cohen, 1997) following 135  
this approach. Berlage proposes CardiAssist, a system 136  
including a simulator for training in echocardiography 137  
(Berlage, 1997). In this clinical application, the typical 138  
problems a trainee has to face are (1) to find the stan- 139  
dard orientations of the probe relatively to the heart, 140  
(2) to detect the relevant anatomical structures in the 141  
images and (3) to learn the diagnostic content of these 142  
features. In this system, slices are computed from a 143  
pre-acquired volume of ultrasonic data and visualised. 144  
A view of a 3D model with visualization of the echo- 145  
graphic plane is offered to the trainee for a better local- 146  
ization of the image. 147

#### 2.1.3. Taking probe pressure into account 148

Further, it is possible to deform the interpolated im- 149  
age obtained with respect to the pressure that is applied 150  
to the probe. The criteria on which this deformation de- 151  
pends on includes important factors such as the arterial 152  
and venous pressure. By modifying these criteria we can 153  
simulate a set of pathologies on which medical students 154  
could be trained for the identification of the latter (Troc- 155  
caz et al., 2000). UltraSim (Aiger and Cohen, 1997) in- 156  
cludes elastic registration tools to build a coherent 157  
volume from data acquired under different probe posi- 158

159 tions therefore involving different local deformations.  
 160 Nevertheless, during simulation no deformation is ap-  
 161 plied onto the images when the computed pressure of  
 162 the virtual probe varies. Varlet (1997) proposes a local  
 163 non-linear model of deformation of the computed image  
 164 allowing to deal with the constraints applied by the tip  
 165 of the echo-endoscope to the local tissues.

166 The simulator we propose is based on the use of an  
 167 interpolation approach to compute realistic echographic  
 168 images in real-time and includes image deformation and  
 169 force rendering using a physical model.

## 170 2.2. Physical modeling

171 However, for a meaningful echographic simulation it  
 172 is of paramount importance to consider the forces in-  
 173 volved in such a procedure since they will dictate the  
 174 deformation of the tissue, and therefore, the subsequent  
 175 image that is acquired.

176 Basdogan et al. (1996) developed an interactive 3D  
 177 model of the human thigh along with a set of surgical  
 178 tools to simulate procedures in virtual environments.  
 179 Laffont (1997) studied the implications of the deforma-  
 180 tion of such a system, which are essential in the develop-  
 181 ment of a realistic simulator coupled to a haptic  
 182 interface. He based his model on a system of inter-con-  
 183 nected springs.

184 Mass-spring networks already been successfully ap-  
 185 plied to areas such as facial animation (Lee et al.  
 186 1995) and have the decisive advantage of being easy-  
 187 to-implement and faster than finite-element simulation  
 188 even though lately considerable speed-ups have been  
 189 achieved in this domain through the use of pre-calcu-  
 190 lated matrices. This has resulted in, for example, the  
 191 real-time simulation with force-feedback of the human  
 192 liver (Bro-Nielsen and Cotin, 1996) based on the *Visible*  
 193 *Human* dataset. However, the model used is inconve-  
 194 nient in the sense that the assumption is made that the  
 195 tissue is hyper-elastic and linear in its deformation. This  
 196 is clearly not the case. As biomechanical experiments  
 197 confirm, the stress-strain curve of human tissue is  
 198 non-linear.

199 Lee et al. (1995) tackles this problem by using a three-  
 200 layer model which takes into account the properties of  
 201 the epidermis, the fatty sub-cutaneous tissue, the muscle,  
 202 and the bone. The great difficulty for such a system lies  
 203 in the identification of the parameters of the individual  
 204 springs that will give the same results to an external  
 205 force being applied as the measurements in the real  
 206 world.

207 On the other hand, in Pai et al. (2001) an interest-  
 208 ing approach is taken; The model is constructed *di-*  
 209 *rectly* from the experimental measurements. The  
 210 model is valid for linear elastic deformations, but is  
 211 unable to take into account non-linear material or  
 212 topology changes.

A complete survey is outside the scope of this paper. 213  
 Hence please refer to d'Aulignac (2001)<sup>1</sup> for a more 214  
 complete review on the real-time simulation of deforma- 215  
 ble objects . 216

## 3. Modeling of the thigh 217

We have constructed a dynamic model of the human 218  
 thigh based on experimental measurements of its elastic- 219  
 ity. The work presented in this section has been done in 220  
 collaboration with Cem Cavesoglu of UC Berkeley in 221  
 the framework of the France-Berkeley cooperation. 222

### 3.1. Experimental setup and data acquisition 223

In order to model an object such that its behavior 224  
 corresponds to reality, measurements must be taken 225  
 on the real object. In this case we are interested in the 226  
 deformation of the thigh with respect to an external 227  
 force which is applied. Intuitively we can affirm that 228  
 the deformation of the thigh is not the same depending 229  
 on the shape of the object used to provoke this deforma- 230  
 tion or more precisely, the contact surface of that ob- 231  
 ject. Since our aim is to build a generic simulation 232  
 which will allow a physically correct behavior which is 233  
 almost independent of the object we choose to deform 234  
 the thigh with, two different objects have been used to 235  
 measure the behavior of the thigh in terms of penetra- 236  
 tion distance with respect to the external force being 237  
 applied. 238

The first of these has a tip of pyramidal shape to pro- 239  
 voke a punctual force response, while the second one 240  
 has the same contact surface area as a typical echo- 241  
 graphic probe. These pseudo-probes are then mounted 242  
 on a force sensor which in turn is mounted on a PUMA 243  
 articulated arm. The probe is then positioned perpendic- 244  
 ularly to the surface of the thigh at each of 64 points 245  
 where measurements will be taken. These points are reg- 246  
 ularly distributed over the area where the echography is 247  
 performed when trying to detect a thrombosis in the 248  
 vein. The robotic arm then advances 2 mm using the ref- 249  
 erence of the end effector, i.e., the probe pushes along 250  
 the axis which is normal to the surface of the thigh at 251  
 the given point. The force is recorded and the procedure 252  
 is repeated up to an upper force limit (Fig. 1). 253

Fig. 2(a) shows the non-linear relationship between 254  
 the penetration distance and the reaction force at 11 dif- 255  
 ferent points along the thigh. The difference in the 256  
 curves may be accounted for due to the fact that the 257  
 thigh is not homogeneous and that the amount of the 258  
 material varies with the location (e.g., in some regions 259  
 fatty tissue might be pre-dominant, while in others there 260

<sup>1</sup> <http://www.aulignac.com/diego/work/publi.html>.

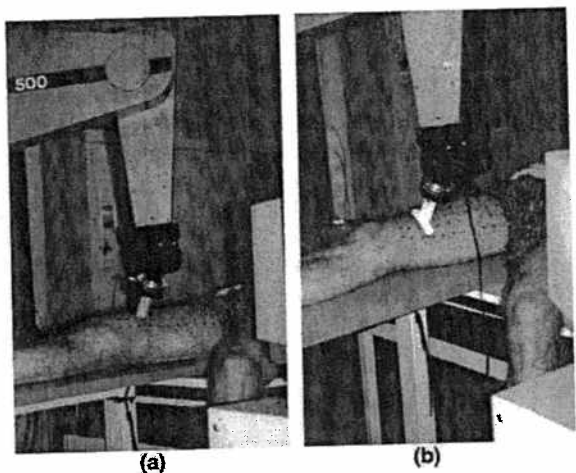


Fig. 1. The two probes used for measuring the behavior of the thigh. A probe with a punctual contact (on the left) and the pseudo-echographic probe with a larger contact surface (on the right).

261 may be very little separating the epidermis from the  
262 bone).

263 Fig. 2(b) plots the values of the forces for the same  
264 points as above but using the second probe with a larger  
265 contact surface. As one might expect this results in a larger  
266 force for the same penetration distance since the  
267 external force applied is distributed over a much larger  
268 area (note that the pressure is defined as force per unit  
269 area).

270 The assumption is that from these two distinct sets of  
271 data it will be possible to make a model which will re-  
272 spond correctly to not only to the two probes used for  
273 measurement purposes, but also other probes of a differ-  
274 ent shape.

275 3.2. Model construction

276 Based on the experimental data and the computa-  
277 tional requirements, a two layer lumped element model  
278 is chosen. Multi-layer models were also used by several

279 authors in the literature, for example in Lee et al.  
280 (1995) for facial animation or in Nebel (2001) for mod-  
281 eling soft tissue with volumetric finite elements.

282 The two layer model is composed of a surface mesh  
283 of masses, linear springs and dampers, and a set of non-  
284 linear springs orthogonal to the surface to model volu-  
285 metric effects by giving normal support to the surface  
286 mesh (see Fig. 3). At each sample point recorded in Sec-  
287 tion 3.1 we place a small mass that is attached to a non-  
288 linear spring. The other end remains fixed (assuming the  
289 bone) at a distance perpendicular to the surface. The  
290 force due to this nonlinear spring is given by  
291

$$f(x) = \frac{x}{ax + b}, \tag{1}$$

294 where  $x$  is the change in length of the spring, i.e., the ac-  
295 tual length minus the initial length. Hence, when  $a$  and  $b$   
296 are positive, the magnitude of the force grows very rap-  
297 idly for  $x < 0$  (i.e., compression).

298 The linear springs on the surface give geometrical as  
299 well as numerical stability to the model. They avoid  
300 any geometrical singularities in the solution as well as

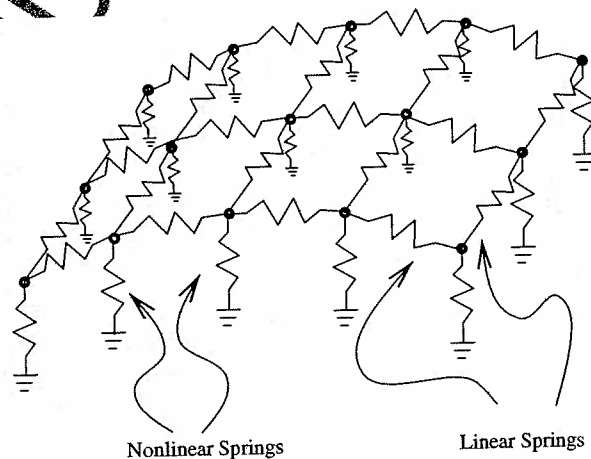


Fig. 3. Two layer model of the thigh.

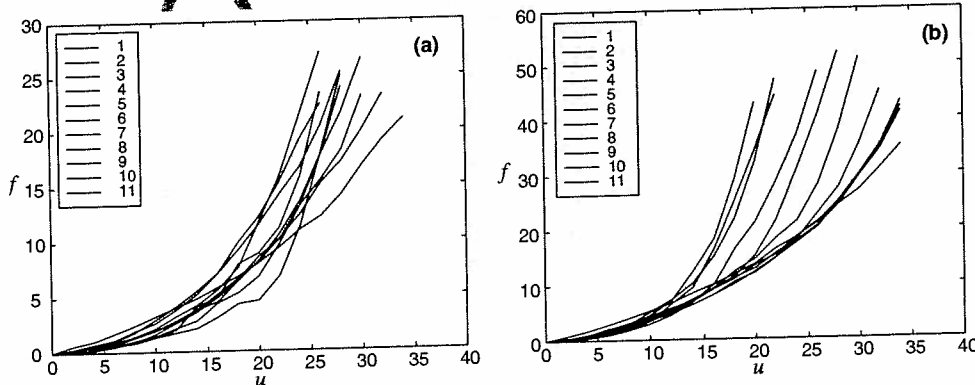


Fig. 2. Plot of the reaction force  $f$  in function of the penetration distance  $u$  at 11 different points on the thigh using a probe with a punctual contact (on the left) and the pseudo-echographic probe with a larger contact surface (on the right).

301 adding damping. The force due to each linear spring is  
302 given by

$$303 \quad f(x) = \lambda x - \mu \dot{x}, \quad (2)$$

306 where  $x$  is the change in length of the spring,  $\lambda$  is the  
307 stiffness and  $\mu$  the damping coefficient. The rate of the  
308 change in length is given by  $\dot{x}$ .

309 The parameters of the surface elements are uniform  
310 whereas the parameters of the nonlinear spring vary  
311 around the mesh to model the heterogeneous nature of  
312 the thigh mentioned above, while keeping the number  
313 of unknown parameters small (d'Aulignac et al., 1999a).

314 It should be noted that this model has been chosen ad  
315 hoc based on the experimental data available of dis-  
316 placement normal to the surface. Hence, its results will  
317 only be valid in compression, but not in extension.

### 318 3.2.1. Parameter estimation

319 Estimation of the model parameters from experimen-  
320 tal measurements is a critical part of the modeling. Sev-  
321 eral types of methods can theoretically be used for  
322 solving this problem: an Artificial Neural Network ap-  
323 proach requiring to make use of an adapted modeling  
324 technique (Szilas and Ronco, 1995), the Simulated  
325 Annealing (Bonomi and Lutton, 1988), the Genetic  
326 algorithms (Goldberg, 1989) which have already given  
327 some good results when identifying the physical param-  
328 eters of a deformable object (see Louchet et al., 1995 and  
329 Joukhadar et al., 1997), and the Steepest Descent meth-  
330 od (Minoux, 1983) which was used for this application.

331 Given that there are 64 sample points, and that at  
332 each point we have taken between 6 and 18 measure-  
333 ments with each probe, we obtain over 1000 different  
334 samples. Our objective is to find the parameters of our  
335 model that best describe this data. We have used a  
336 two step optimization approach based on nonlinear  
337 least squares estimation.

- 338 1. The experimental data of the indenter is first fit to a  
339 simple model without any surface elements, i.e., only  
340 the nonlinear springs.
- 341 2. The results of the previous fit is used as the initial  
342 conditions for the parameter estimation of the com-  
343 plete model; the parameters of the surface and non-  
344 linear springs are adjusted in order to best match  
345 the experimental data of the indenter and the  
346 pseudo-echographic probe.

347  
348 This approach is chosen to avoid problems with local  
349 minima. We have obtained better results with this meth-  
350 od than using genetic algorithms, perhaps, as the num-  
351 ber of parameters is small, while genetic algorithms are  
352 usually better suited for problems involving large num-  
353 bers of unknowns.

354 One thing to note here is that the parameter estima-  
355 tion is based on a simplified interaction model between  
356 the tissue and probe, making the assumption that the in-  
357 denter will principally act on one spring since the con-  
358 tact area is small, while the larger probe acts on three  
359 nodes simultaneously. In this simplified interaction  
360 model, the nodes that are not in contact with the probe  
361 are kept stationary. This is a valid assumption for the  
362 thigh, as deformations are very local.

363 The mean absolute error between the measured val-  
364 ues and the values estimated by the model is 1.05 N,  
365 with standard deviation of 0.84 N, over the whole dataset  
366 (i.e., all measurement samples obtained with both  
367 probes). This is equivalent to an average error of 5%.  
368 The distribution of the error can be seen in Fig. 4, show-  
369 ing how many of the values estimated by the model ex-  
370 hibit a given error with respect to the real measurements.

371 The few cases that give very large errors are due to  
372 inaccuracies in the measurements at some of the sample  
373 points (probably due to movement of the leg during the  
374 process). For these points there exist no parameters  
375 allowing a smooth interpolation of the data, thus result-  
376 ing in large errors. Fortunately the extent of this phe-  
377 nomenon is limited.

### 378 3.2. Graphical model

379 The area of the thigh of interest for an echographic  
380 exam is relatively small as compared to the whole leg.  
381 Thus it is sufficient to model the deformation only in this  
382 area. However, to give the user an increased sense of  
383 realism and as landmarks for orientation in the virtual  
384 environment, we also render the lower leg and other side  
385 of the thigh. These are not deformable and thus the po-  
386 sition of the vertexes will not change during simulation.  
387 It is therefore possible to transfer this data only once to

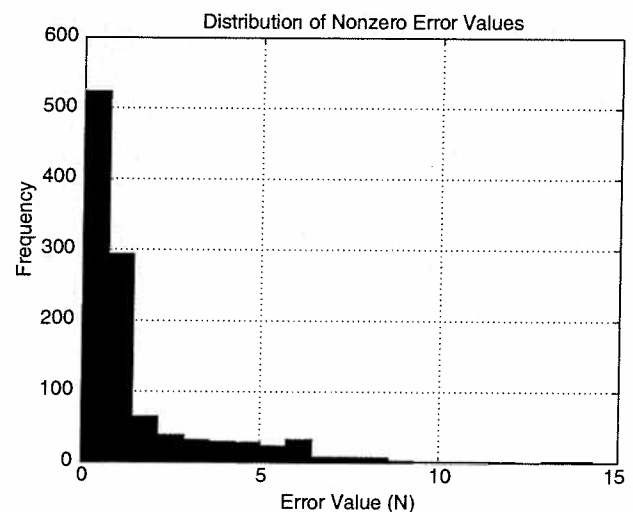


Fig. 4. Frequency distribution of the error between the measured values and the values estimated by the model.

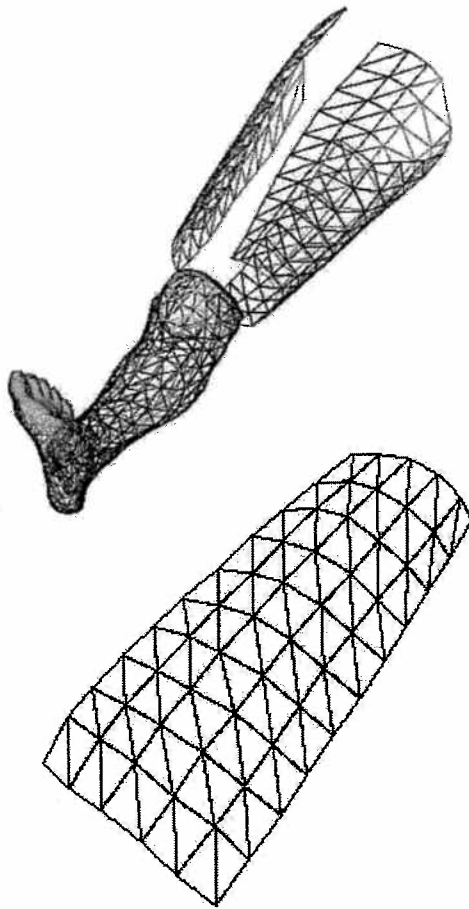


Fig. 5. Decomposition of the parts of the leg (right). The part on the left is the only part where deformation is simulated.

388 the graphics hardware, and subsequently it will put only  
389 minimal demands on the CPU.

390 Fig. 5 shows how the area where deformation is sim-  
391 ulated is integrated with the rest of the components that  
392 represent the leg only graphically. Only the linear  
393 springs on the surface are shown; the nonlinear springs  
394 are not visible in the graphical output.

#### 395 4. Dynamic resolution

396 As discussed in Hairer and Wanner (1991), explicit  
397 integrations suffers from stability problems. This means  
398 that for a given timestep there is a restriction on the  
399 physical parameters that allow a stable integration.  
400 Moreover, the larger the stiffness, the smaller the time-  
401 step must be, when using explicit methods.

402 The stiffness values that we have estimated in Section  
403 3.2.1 are such that the integration is not stable on our  
404 computer unless artificially large inertial values are used,  
405 i.e., large mass. This, however, leads to an unnaturally  
406 slow reaction to an external force that is applied. Fur-  
407 ther the implementation of gravitational forces is impos-

sible. Even, higher order methods explicit methods do  
not allow us increase speed since the stability region  
does not double as we double the number of stages  
per timestep.

#### 4.1. Implicit integration

Unsatisfied with explicit integration for our simula-  
tion, we have decided to investigate the suitability of im-  
plicit methods. Since speed rather than accuracy is our  
main concern, we have opted for the *semi-implicit* Euler  
method (Eq. (3)) having excellent stability (see Baraff  
and Witkin, 1998). For each step in the simulation the  
forces on the mass-points are calculated and the linear  
system is solved using the conjugate gradient method

$$\Delta y \left[ \frac{1}{h} I - \frac{\partial f}{\partial y} \right] = f(y_0), \quad (3)$$

where  $y$  is the state vector expressing the positions and  
velocities of all particles. Thus  $\Delta y$  represents the change  
in state and  $f(y_0)$  the derivative at the current state. Fur-  
ther,  $I$  is the identity matrix and  $\partial f / \partial y$  the Jacobian ma-  
trix. The accuracy of the solution is proportional to the  
timestep  $\Delta t$ . Higher order integration will yield better  
accuracy, the implicit midpoint method, for example,  
has a consistency of  $O(h^2)$ , but at a higher computa-  
tional cost.

Since we only solve the linear system once per time-  
step, our resolution is only semi-implicit and not guar-  
anteed to be stable for any timestep, however, it is  
much faster to solve and has not given us stability prob-  
lems in practice.

#### 4.2. Experimental results

Fig. 6 shows the model as it has been built in our sim-  
ulation system. A force is being applied on the thigh  
using a probe which provokes a deformation which is  
in accordance with the measurements taken. The com-  
putational speed on a Silicon Graphics R10000 machine



Fig. 6. Dynamic deformation of the thigh under pressure.

444 is in the order of 100 timesteps per second of animation  
 445 using semi-implicit integration, which lets us envisage  
 446 our simulation system as part of a working echographic  
 447 simulator which operates in real-time (d'Aulignac et al.,  
 448 1999b).

449 **5. Interaction**

450 In the previous sections the deformation of the thigh  
 451 has been modeled. In this section we shall examine how  
 452 to interact with the model we created using a virtual ech-  
 453 ographic probe. In Section 5.1 the collision detection  
 454 and response are discussed while the haptic force-feed-  
 455 back interface is detailed in Section 5.2.

456 **5.1. Collision detection and response**

457 The virtual echographic probe we use to interact with  
 458 the model of the thigh is simple in shape, and can be  
 459 modeled as a parallelepiped. However, the surface of  
 460 the thigh is represented by many polygons and can be-  
 461 come concave during interaction.

462 Therefore we choose to use the approach by Lom-  
 463 bardo et al. (1999). Hence, to find the triangles of the  
 464 thigh in collision with the probe, we render the surface  
 465 (enabling the picking mode) in a orthogonal bounding  
 466 box equivalent to the shape of the tool. This returns  
 467 the polygons inside the tool, i.e., in collision.

468 **5.1.1. Distance computation**

469 Finding the polygons of the thigh in interaction with  
 470 the tool will not automatically compute the distance. We  
 471 make the assumption that the tool is touching the thigh  
 472 using the front side of the parallelepiped. Hence the in-

ter-penetration distance is computed as the distance be- 473  
 tween a polygon and the front tip of the tool. 474

5.1.2. Collision forces 475

If an inter-penetration distance has been found a 476  
 non-linear penalty force is calculated according to Deg- 477  
 uet et al. (1998). This force is then distributed over the 478  
 three particles of the colliding polygon using the bary- 479  
 centric coordinates of the point on the triangle closest 480  
 to the tip of the tool. 481

5.2. Haptic interaction 482

In Section 4 we have seen that our simulation runs at 483  
 approximately 100 Hz on an SGI Octane 175 Hz. This 484  
 means that we check one-hundred times for the collision, 485  
 calculate the appropriate penalty for a penetration (if 486  
 present), and update the position of the vertexes of the 487  
 deformable area according to external and internal 488  
 forces each second. Even if this guarantees a stable sim- 489  
 ulation visually, i.e., at least 10 frames a second, haptic 490  
 force feedback may be unsatisfactory. By this we mean 491  
 that as the contact forces are transmitted to the PHAN- 492  
 Tom (distributed by SensAble Technologies) at the men- 493  
 tioned simulation rate, unacceptable trembling may 494  
 result to the low frequency of the force update. Balaniuk 495  
 (1999) proposes the use of a local approximation of the 496  
 contact which we shall use in this application (Fig. 7). 497

5.2.1. Experimental results 498

As mentioned in the previous chapter, interaction 499  
 forces with the simplified model are much less costly 500  
 to evaluate, and therefore, can be calculated at a much 501  
 higher frequency that will give a much smoother force 502  
 feedback response. Fig. 9 shows the user interactively 503  
 deforming the surface of the thigh. 504

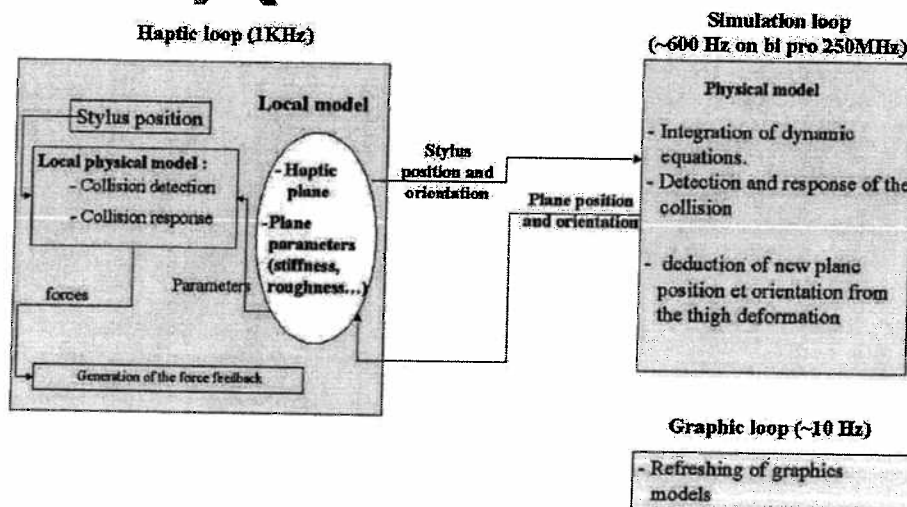


Fig. 7. Graphical overview of the two threads: the force feedback (on the left, running at 1 kHz) and the simulation (on the right).

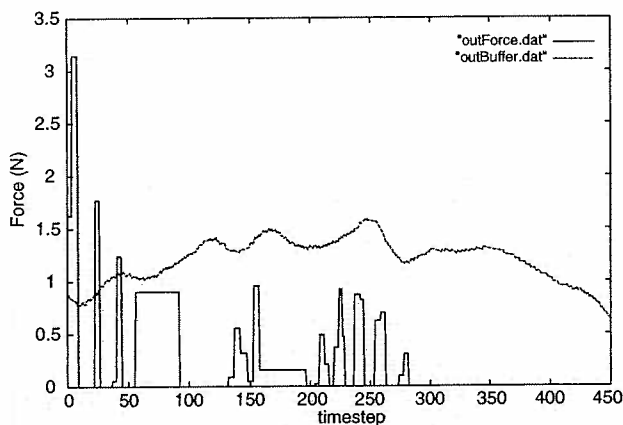


Fig. 8. Evolution of the force over a time interval using the haptic buffer model (dashed), and without (solid).

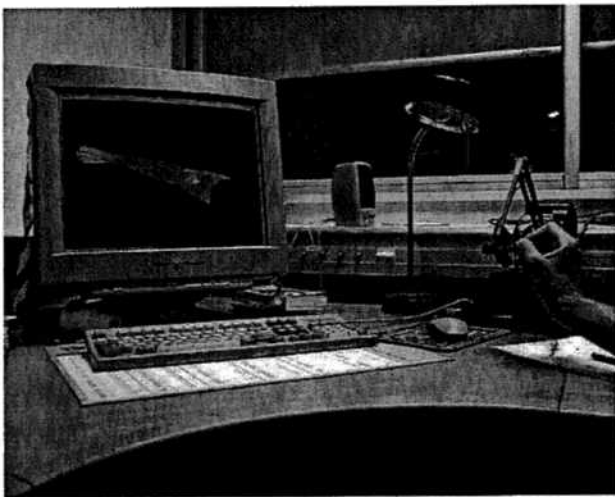


Fig. 9. The thigh model manipulated by the phantom.

505 Fig. 8 shows the evolution of the magnitude of the  
 506 force during a manipulation of the virtual thigh. Using  
 507 the virtual probe we touch the thigh and slide over the  
 508 surface. When using the buffer model we obtain the  
 509 dashed curve. However, when attempting similar inter-  
 510 action without the buffer model we obtain the solid  
 511 curve. This curve presents serious discontinuities; when  
 512 forces return to a zero value the user has lost contact  
 513 with the surface of the thigh due to the trembling. This  
 514 trembling is due to the large variation of the forces  
 515 (d'Aulignac et al., 2000).

#### 516 5.2.2. Discussion

517 The local model we have implemented is a static  
 518 approximation of the *contact*. By this we mean that col-  
 519 lision detection and response are calculated using a sim-  
 520 plified geometrical model at a much higher frequency  
 521 using a multi-threaded architecture. However, the *defor-*  
 522 *mation* is not modeled; the local model's parameters are

constant during one step of the physical simulation (the  
 latter calculating deformation and global collision  
 detection).

Therefore, an interesting extension of the presented  
 approximation the contact, would be to combine it with  
 low order models of the deformation such as presented  
 in Cavusoglu and Tendick (2000) or Astley and Hay-  
 ward, 1998.

## 6. Echographic image generation

As a pedagogical tool our simulator described so far  
 is sterile. Images corresponding to the actual deforma-  
 tion must be generated to teach practitioner the *correla-*  
*tion* between deformation of the surface of the thigh and  
 the resulting echographic image. Hence for any position  
 and orientation of the probe on the surface of the thigh  
 we must generate an image. Since we can not acquire  
 nor store an infinite amount of images for all points  
 we will have to resort to some kind of interpolation tech-  
 nique. However, we must first prepare the data.

To collect this data we have taken echographic  
 images at the same point as we have measured force-dis-  
 placement curves. These echographic slices are then ar-  
 ranged within a bounding box (see Fig. 10) which will  
 be divided into a 3D voxel map. The voxel map is then  
 filled depending on the intensity of the pixels of the ech-  
 ographic images within each voxel. These voxels are of  
 equilateral shape, and their size is chosen with respect  
 to the available live memory on the machine (i.e., no  
 swap).

*Voxel map size.* In this case we have used a voxel size  
 of 0.3 mm leading to a memory requirement of approx-  
 imately 120 Mb. Since the resolution of one pixel on the  
 original echographic images is 0.1 mm there will be a  
 small loss in resolution due to memory limitations.

*Interpolation.* It is clear that the for the number of  
 sample images we have acquired the voxel map will be

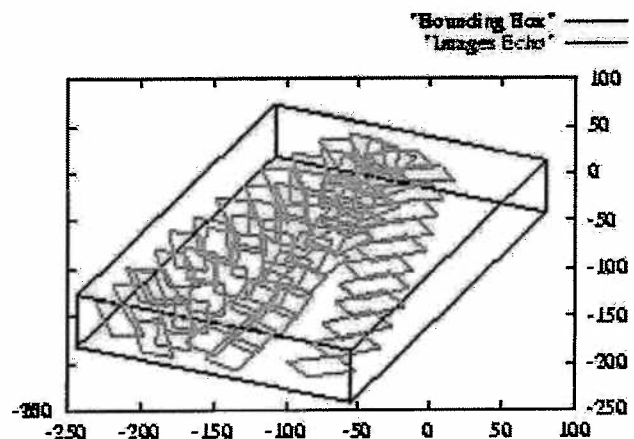


Fig. 10. Echographic slices arranged in a 3D volume.



559 far from full. To fill the blank voxels we use interpola-  
 560 tion. The TIMC laboratory has provided us with such  
 561 an interpolation tool within the framework of a collab-  
 562 oration. Thus the voxel map is filled in the preprocessing  
 563 stage once and, thereafter, slices through the voxel map  
 564 may be generated in real-time. The resolution of the gen-  
 565 erated image is, of course, dependent on the resolution  
 566 of the voxel map (Vieira, 2000).

567 Once the voxel map is filled, we may calculate an im-  
 568 age for any given position and orientation on the mod-  
 569 eled area of the thigh. Given the data can be stored in  
 570 live memory this procedure is performed in real-time.

### 571 6.1. Image deformation

572 *Motivation.* The images to construct the voxel map  
 573 where acquired without deformation: the echographic  
 574 probe was placed on the sample point and minimal pres-  
 575 sure was applied to obtain the echographic image.  
 576 Hence an image generated from the voxel map will be  
 577 non-deformed. However, to detect a thrombosis in the  
 578 thigh, the diagnosis is based on the deformation of vein.  
 579 It is therefore essential for a useful simulator to take this  
 580 phenomenon into account.

581 *Problem statement.* The main difficulty in modeling  
 582 the deformation lies in the fact that each structure has  
 583 its own way of reacting under pressure. Arteries have al-  
 584 most no deformation while non-pathological veins flat-  
 585 ten. Superficial soft tissues have a near linear  
 586 deformation. Deep tissues and bones have negligible  
 587 deformation (Troccaz et al., 2000).

588 *Existing approaches.* The deformation of the image  
 589 when pressure is applied can be obtained through the

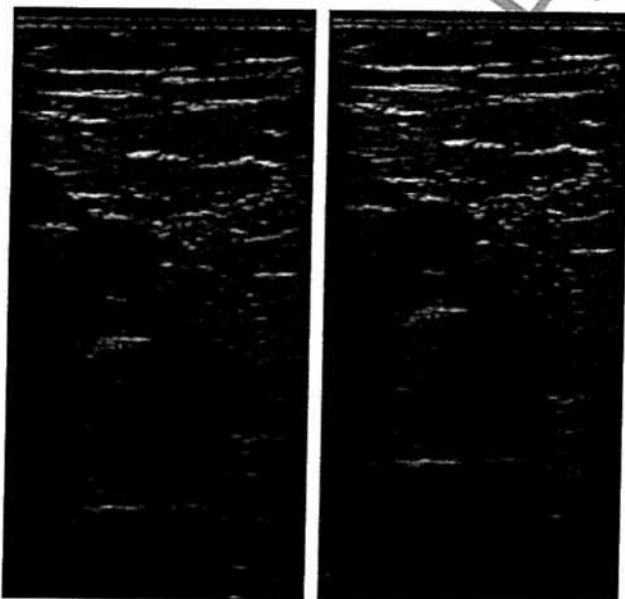


Fig. 11. Echographic images generated for a given location and orientation, with (right) and without (left) deformation.



Fig. 12. On-line generation of echographic images when interacting with the thigh using the force-feedback device. A video can be downloaded from <http://www.aulignac.com/diego/work/publi.html>.

590 approach of Henry (1997). Given a segmentation of  
 591 the undeformed echographic image to find the artery,  
 592 vein and soft tissue areas their deformation can be cal-  
 593 culated by taking into account parameters such as arte-  
 594 rial and venous pressure. As mentioned before, by  
 595 modifying these criteria we can simulate a set of pathol-  
 596 ogyes. Alternatively, a deformation function can be cal-  
 597 culated directly from the position of features on a  
 598 deformed and undeformed image. However, both these  
 599 approaches rely on a segmentation having been per-  
 600 formed previously.

601 Since our voxel map is not segmented into the differ-  
 602 ent anatomical structures we have momentarily adopted  
 603 a linear deformation regardless of the tissue. Therefore,  
 604 future work on this subject should examine this problem  
 605 in detail; a possibility might be to use precalculated  
 606 deformation functions as described in Troccaz et al.  
 607 (2000).

### 608 6.2. Experimental results

609 Fig. 11 shows how the echographic image changes as  
 610 an increasing pressure is applied to the surface of the  
 611 thigh by the means of the virtual echographic probe.  
 612 The probe's position is given by the force-feedback de-  
 613 vice (see Fig. 12).

## 614 7. Conclusions

615 In this paper we have described the building blocks to  
 616 prototype of an echographic simulator.

617 Measurements have been taken on a real human  
 618 thigh using an articulated robot arm in combination  
 619 with a force sensor. The force-displacement curves we  
 620 have obtained on different sample points on the thigh

621 demonstrate both the non-linear and non-homogeneous  
622 elastic nature of the material.

623 Furthermore, we have built a mass-spring model of  
624 the area of the thigh where the measurements were taken.  
625 The topology of this model is based on the position of  
626 the sample points and by making assumptions on the  
627 anatomy based on the experimental data acquired.  
628 Hence, we have chosen a layered model with non-linear  
629 springs that approximate the measured force-displace-  
630 ment behavior. As the elasticity of the thigh is non-  
631 homogeneous a protocol of parameter identification  
632 has been installed. Using a method of steepest descent  
633 we aim to represent *all* the data samples with the lowest  
634 possible error.

635 To model the dynamics we have investigated the use  
636 of both explicit and implicit methods. We come to the  
637 conclusion that the overhead of solving a linear system  
638 at each time step using a semi-implicit integration is  
639 preferable to explicit integration. Because of the stiffness  
640 of the springs the latter approach is obliged to take ex-  
641 tremely small timesteps to maintain stability.

642 To calculate the collision response we use the distance  
643 of penetration as a measure to calculate the penalty  
644 based response forces. However, if these forces are sup-  
645 plied to the force-feedback device at the rate of the phys-  
646 ical simulation of the deformation (100 Hz using semi-  
647 implicit integration with constant Jacobian), unaccept-  
648 able trembling will be the result. To remedy this problem  
649 we apply a local approximation of the contact, that will  
650 calculate the collision forces at a much higher rate (e.,  
651 1 kHz) in a separate program thread. This process suf-  
652 fices to largely improve the haptic sensation.

653 Lastly we have integrated our physical model with a  
654 generator of echographic images. Previous methods  
655 have interpolated images along one privileged direction  
656 of the thigh (namely the direction of the vein). Since, in  
657 this case, we want to provide an image at any position of  
658 the modeled area, we have created a voxel map based  
659 approach. The echographic images acquired at the sam-  
660 ple points are used to partially fill the voxel map; using  
661 interpolation we then obtain a full 3D representation of  
662 the echographic data. From this voxel map, echographic  
663 images at any position or orientation can be found.

664 The components of the simulator have been success-  
665 fully integrated in this first version. We have demon-  
666 strated that a real time production of deformable  
667 realistic echographic images and corresponding tactile  
668 feedback was possible. The following stage of this pro-  
669 ject will be its clinical testing; this means that lessons  
670 must be designed and implemented on the basis of the  
671 existing simulator to allow a beginner to experiment ech-  
672 ographic examination and diagnosis with the simulator.  
673 The comparison of performances of learners using the  
674 simulator versus learners using traditional learning is  
675 the next stage and should demonstrate the potentiality  
676 of such tools.

## Acknowledgements

We thank Cenk Cavosuglu who has been actively in-  
volved in the development of the mass-spring model of  
the thigh as well as the France-Berkeley Fund that made  
this cooperation possible. Further, we thank Etienne  
Dombre and Francois Pierrot at the LIRMM labora-  
tory (Montpellier, France) for their kind assistance  
while taking the measurements at their lab. Also many  
thanks to Remis Balaniuk who developed the local mod-  
el, and Ivan Costa for the interesting scientific discus-  
sions about the project.

## Appendix A. Supplementary data

Supplementary data associated with this article can  
be found, in the online version at doi:10.1016/  
j.media.2005.02.001.

## References

- Aigen, D., Cohen, D., 1997. Real-time ultrasound imaging simulation. *RTI* 693  
694
- Astley, Q., Hayward, V., 1998. Multirate haptic simulation achieved  
by coupling finite element meshes through Norton equivalents. In:  
Proceedings of the IEEE International Conference on Robotics  
and Automation, Leuven, BE, pp. 989-994. 695  
696  
697  
698
- Balaniuk, R., 1999. Using fast local modeling to buffer haptic data. In:  
Proceedings of the Fourth Phantom User Group Workshop -  
PUG99, Boston, US. 699  
700  
701
- Bamber, J., Dickinson, R., 1986. Ultrasonic b-scanning: a computer  
simulation. *Physics in Medicine and Biology*. 702  
703
- Baraff, D., Witkin, A., 1998. Large steps in cloth simulation. In:  
Cohen, M. (Ed.), SIGGRAPH 98 Conference Proceedings, Annual  
Conference Series, ACM SIGGRAPH. Addison Wesley, pp. 43-  
54. 704  
705  
706  
707
- Basdogan, C., Loan, P., Rosen, J.M., Delp, S., 1996. An interactive  
model of the human thigh for simulating surgical procedures in  
virtual environments. *Advances in Bioengineering ASME*. 708  
709  
710
- Berlage, T., 1997. Augmented reality for diagnosis based on ultra-  
sound images. *Proceedings of CVRMed-MRCAS'97, LCNS Series*,  
vol. 1205. Springer Verlag, pp. 253-262. 711  
712  
713
- Bonomi, E., Lutton, J.-L., 1988. Le recuit simulé. *Pour la science*, 68-  
77. 714  
715
- Bro-Nielsen, M., Cotin, S., 1996. Real-time volumetric deformable  
models for surgery simulation using finite elements and condensa-  
tion. In: *Proceedings of Eurographics*, vol. 15, pp. 57-66. 716  
717  
718
- Cavosuglu, M., Tendick, F., 2000. Multirate simulation for high  
fidelity haptic interaction with deformable objects in virtual  
environments. In: *IEEE International Conference on Robotics  
and Automation, ICRA 2000, San Francisco*. 719  
720  
721  
722
- d'Aulignac, D., 2001. Modélisation de l'interaction avec objets  
déformables en temps-réel pour des simulateurs médicaux. PhD  
thesis, Institut National Polytechnique de Grenoble. Available  
from: <<http://www.aulignac.com/diego/work/publi.html>> (in  
English). 723  
724  
725  
726  
727
- d'Aulignac, D., Balaniuk, R., Laugier, C., 2000. A haptic interface for  
a virtual exam of the human thigh. In: *Proceedings of the IEEE  
International Conference on Robotics and Automation*, vol. 3, San  
Francisco, CA, US, pp. 2452-2457. 728  
729  
730  
731

677

678

679

680

681

682

683

684

685

686

687

688

689

690

691

692

693

694

695

696

697

698

699

700

701

702

703

704

705

706

707

708

709

710

711

712

713

714

715

716

717

718

719

720

721

722

723

724

725

726

727

728

729

730

731

- 732 d'Aulignac, D., Cavusoglu, M.C., Laugier, C., 1999a. Modelling the  
733 dynamics of a human thigh for a realistic echographic simulator  
734 with force feedback. In: Proceedings of the International Confer-  
735 ence on Medical Image Computer-assisted Intervention, Cam-  
736 bridge, UK.
- 737 d'Aulignac, D., Laugier, C., Cavusoglu, M.C., 1999b. Towards a  
738 realistic echographic simulator with force feedback. In: Proceed-  
739 ings of the IEEE-RSJ International Conference on Intelligent  
740 Robots and Systems, vol. 2, Kyongju, KR, pp. 727-732.
- 741 Deguet, A., Joukhadar, A., Laugier, C., 1998. A collision model for  
742 deformable bodies. In: IEEE International Conference on Intelli-  
743 gent Robots and Systems.
- 744 Goldberg, D.E., 1989. Genetic Algorithms in Search, Optimization  
745 and Machine Learning. Addison-Wesley.
- 746 Hairer, E., Wanner, G., 1991. Solving Ordinary Differential Equations  
747 II. Springer-Verlag, Berlin.
- 748 Henry, D., 1997. Outils pour la modélisation de structure et la  
749 simulation d'examsens échographiques. PhD thesis, Université  
750 Joseph Fourier, Grenoble, FR (in French).
- 751 Jensen, J., 1996. Field: A program for simulating ultrasound systems.  
752 In: 10th North-Baltic Conference on Biomedical Imaging, pp. 351-  
753 353.
- 754 Joukhadar, A., Garat, F., Laugier, C., 1997. Constraint-based  
755 identification of a dynamic model. In: Proceedings of the IEEE-  
756 RSJ International Conference on Intelligent Robots and Systems,  
757 Grenoble, FR.
- 758 Laffont, P., 1997. Simulation Dynamique Pour Le Diagnostic De  
759 Thromboses Veineuses. Mémoire De Diplôme D'études Appro-  
760 fondies. Université de Savoie, Chambéry, FR.
- 761 Lee, Y., Terzopoulos, D., Waters, K., 1995. Realistic facial modeling  
762 for animation. In: Computer Graphics Proceedings, Annual  
763 Conference Series, Proc. SIGGRAPH '95, Los Angeles, CA,  
764 ACM SIGGRAPH, pp. 55-62.
- 765 Lombardo, J.-C., Cani, M.-P., Neyret, F., 1999. Real-time collision  
766 detection for virtual surgery. In: Computer Animation, Geneva,  
767 Switzerland.
- Louchet, J., Provot, X., Crochemore, D., 1995. Evolutionary identi- 768  
fication of cloth animation models. In: Computer Animation and 769  
Simulation. Proceedings of the Eurographics Workshop. 770
- Meunier, J., 1989. Analyse des textures d'échocardiographie bidimen- 771  
sionnelles du myocarde. PhD thesis, Université de Montreal (in 772  
French). 773
- Minoux, M., 1983. Programmation mathématique - Théorie et 774  
algorithmie. Collection Technique et Scientifique des Télécommu- 775  
nications, Dunod. 776
- Nebel, J.-C., 2001. Soft tissue modelling from 3d scanned data. In: 777  
Magenat-Thalmann, N., Thalmann, D. (Eds.), Deformable Ava- 778  
tars. Kluwer, pp. 85-97. 779
- Pai, D.K., van den Doel, K., Jamet, D.L., Lang, J., Lloyd, J.E., 780  
Richmond, J.L., Yau, S.H., 2001. Scanning physical interaction 781  
behavior of 3D objects. In: Computer Graphics (ACM SIG- 782  
GRAPH 2001 Conference Proceedings). 783
- Szilas, N., Ronco, E., 1999. Action for learning in non-symbolic 784  
systems. In: European Conference on Cognitive Science, Saint 785  
Malo, France. 786
- Troccaz, J., Henry, D., Laib, N., Champleboux, G., Bosson, J.L., 787  
Pichot, O., 2000. Simulators for medical training: application to 788  
vascular ultrasound imaging. Journal of Visualization and Com- 789  
puter Animation. 790
- Varlet, E., 1997. Etude d'un simulateur pédagogique d'écho-endosco- 791  
pie digestive: modélisation et réalisation. PhD thesis, Université 792  
Sciences et Techniques de Lille (in French). 793
- Vieira, S., 2000. Intégration de modèles déformables avec un 794  
générateur d'images échographiques. Technical report, Diplome 795  
d'Ingénieur, Conservatoire National des Arts et Metiers (in 796  
French). 797
- Wibaix, L., Varlet, E., Chaillou, C., 1997. Construction d'images 798  
échographique pour des simulateurs médicaux. In: Seme Journées 799  
AFIG 97. 800  
801

UNCORRECTED PROOF

